nature materials

SUPPLEMENTARY INFORMATION

DOI: 10.1038/NMAT3923

Hydrogen-bonded structure and mechanical chiral response of a silver nanoparticle superlattice

Bokwon Yoon[1], W. D. Luedtke[1], Robert N. Barnett[1], Jianping Gao[1], Anil Desireddy[2], Brian E. Conn[2], Terry Bigioni[2], and Uzi Landman[1*]

[1] School of Physics, Georgia Institute of Technology, Atlanta, GA 30332-0430, USA

[2] Department of Chemistry and School of Solar and Advanced Renewable Energy, University of Toledo, Toledo, OH 43606, USA

S.1 (a) Variations in the structure of the metal core of the Na_4Ag_{44} (p-MBA)$_{30}$ nanoparticle, between the isolated monomer and when embedded in the nanoparticle superlattice (b) Intrar\layer (L_2) and interlayer (L_3) binding between neighboring nanopaerticles

S.2 Volume compression calculations of the naoparticle superlattice

S.3 The Birch equation of state (EOS)

S.4 Compression-induced changes in the structure of Na_4Ag_{44} (p-MBA)$_{30}$ in the NPSL

S.5 Intralayer and interlayer nanoparticle rotations

S.6 Torsion angles plotted versus the compression parameter V/V_0

S.7 Calculation of cluster rotations (Fig. 3(j))

DOI: 10.1038/NMAT3923

S.1
(a) Variations in the structure of the metal core of the Na_4Ag_{44} (p-MBA)$_{30}$ nanoparticle, between the isolated monomer and when embedded in the nanoparticle superlattice

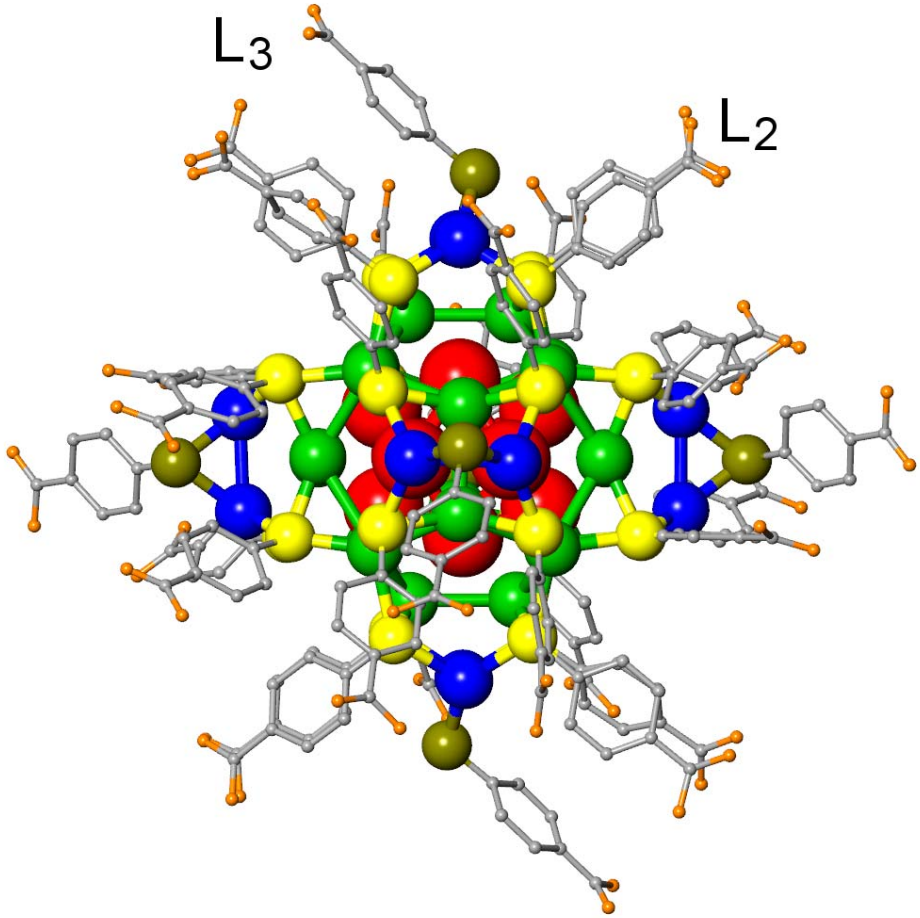

Figure S1(a)

Figure S1(a): Optimal structure of the Na_4Ag_{44} (p-MBA)$_{30}$ nanoparticle showing silver core and p-MBA ligands (see below for colour scheme); the four Na atoms are not shown. The doubly-bundled (L_2) and triply-bundled (L_3) bonded to one of the Ag_2S_5 mounts (at the top) are marked. Colour scheme: red - inner 12 Ag empty-core icosahedron; green –

20 Ag atom dodecahedron; yellow – sulfur atoms in the mounts (4 S atoms in each mount forming an approximate square); grey – carbon; orange – oxygen; blue – exterior 12 Ag atoms in the mounts (2Ag per mount); dark gold – bridging sulfur atoms in the mounts (1 S atom per mount bridging the 2 Ag (blue) atoms).

TABLE S1. Average and standard deviations(in parenthesis) of the radial distances of the metals core atoms organized in shells in the Na_4Ag_{44} (p-MBA)$_{30}$ nanoparticle (NP) : the three silver shells are given in red, green and blue in Fig. S1(a). We show results for the isolated (monoer) Na_4Ag_{44} (p-MBA)$_{30}$ NP), and for the NP as part of the superlattice (NPSL). In both cases the radial distances are calculated with reference to the center of mass of the inner 12 Ag atom empty icosahedral core of the NP. The different shells are indicated in the leftmost column. In the 2nd and 3rd columns we give the average change in the radial distance of the shells, and the actual atomic displacement that occur when comparing the values for the shells of atoms of the NP in the NPSL with the corresponding values for the isolated NP. The values in this Table were obtained for the NPs by starting from their x-ray-determined coordinates with subsequent optimization using conjugated gradients in conjunction with first-principles DFT calculations.

SHELL	radial distance change (Å)	Displacement (Å)	radial distance in superlattice (Å)	radial distance in monomer (Å)
Ag_{12} core	0.0009 (0.0089)	0.0160 (0.0063)	2.7462 (0.0237)	2.7471 (0.0274)
Ag_{20} inner shell	0.0016 (0.0088)	0.0334 (0.0129)	4.5471 (0.0316)	4.5487 (0.0332)
outer 12 Ag atoms	-0.0127 (0.0172)	0.0453 (0.0225)	6.6667 (0.0388)	6.6540 (0.0447)

DOI: 10.1038/NMAT3923

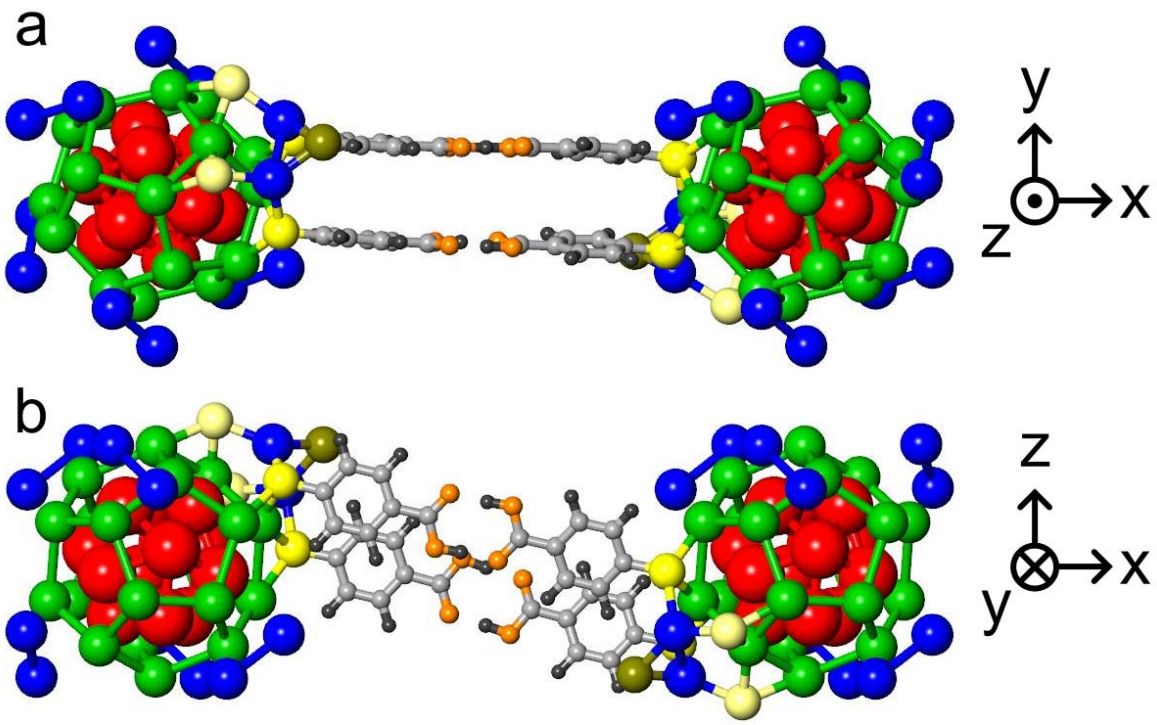

Figure S1(b) intralayer L_2 binding

Figure S1(b): Two views (a and b) of the p-MBA ligand-ligand binding between two neighboring silver nanoparticles, both located in the same layer of the superlattice. The hydrogen-bonded doubly-bundled ligands (L_2) are anchored through two of the S atoms of the mounts.; the sulfur atoms of the Ag_2S_5 mount of the nanoparticels participating in the binding are shown, while they are omitted for the other mounts for clarity. Note the high degree of parallel orientation between the ligands in the bundles, and the stretched conformation of the p-MBA molecule. The color scheme is as in Fig. S1(a).

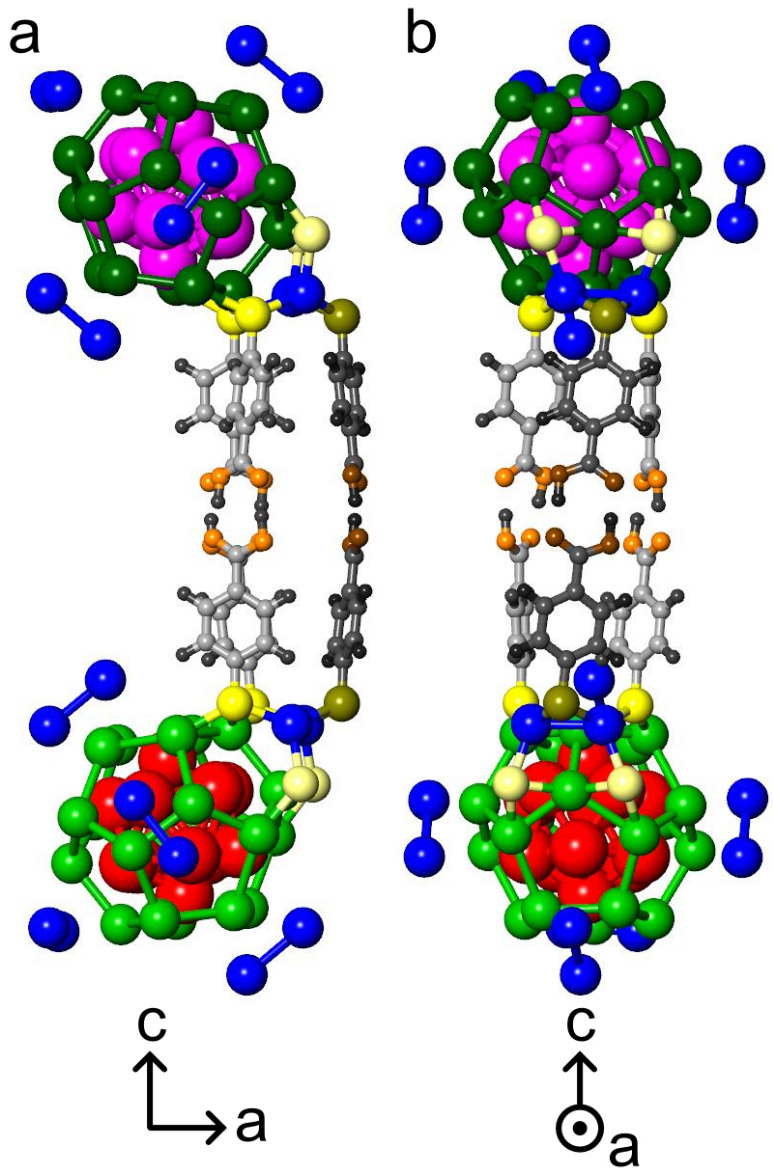

Figure S1(c) interlayer L_3 binding

Figure S1(c). Two views (a and b) of the p-MBA ligand-ligand binding between two neighboring silver nanoparticles, located in neighboring layers of the superlattice (the Ag_{12} icosahedral inner core is colored red in one of the layers and pink in the other); the two clusters are mirror reflection of each other . The hydrogen-bonded triply-bundled ligands (L_3) are anchored through three of the S atoms of the mount – two of the S atoms (colored yellow) are part of the 4S squate, and the third S is located at the apex of the mount (colored dark gold); the sulfur atoms of the Ag_2S_5 mount of the nanoparticels participating in the binding are shown, while they are omitted for the other mounts for clarity. The tri

DOI: 10.1038/NMAT3923

S.2 Volume compression calculations of the nanoparticle superlattice

In the first-principles DFT calculations of the total energy of the NPSL during a hydrostatic volume compression process we started from an optimized configuration of the triclinic unit cell of the NPSL (containing two Na_4Ag_{44} (p-MBA)$_{30}$ nanoparticles); this optimized configuration was obtained from a relaxation of the x-ray determined structure. The relaxation preserved the experimental shape and c/a ratio ((=1.610), and the optimized (minimum total energy) configuration was found to have a length-scale that is 1.00% larger than the experimental one (the optimized unit cell volume was found to be V_0 = 24558.456 Å^3, i.e. 3.02% larger than the experimental one).

In the simulation of the compression we preserved the shape and the c/a ration (1.610) and each step-reduction in the volume from the previous one was achieved by scaling the position vectors in the unit cell by a scaling factor ζ_n <1, so that the volume in the nth compression step was $V_n = \zeta_n^3 V_0$. Subsequent to the scaling of the distances, the atomic configuration for the compressed NPSL was optimized using conjugate gradients in conjunction with the first-principles DFT evaluation of the total energy.

In order to test the adequacy of our assumption of constraining the c/a ratio to remain constant (1.610) throughout the compression process, we have performed several calculation where we determined for selected values of V/V_0 the value of c/a that minimizes the total energy of the NPSL.

We show below results of such calculations for four selected values of V/V_0 :

V/V_0=0.9707 (in the middle of the low strain region, see Fig. 2a in the manuscript).

V/V_0=0.9497 (3 compression steps before the end of low strain, LS, region).

V/V_0=0.9439 (end of the low strain region), and

V/V_0=0.8368 (in the middle of the high strain, HS, region).

In the Table we show the energies calculated for the four selected points both for the constrained c/a calculations and for the ones where c/a was allowed to vary (the latter denoted as E_{min}). We also display the cluster rotation angle, obtained with ((θ_{rot}(1.610)) and without ($\theta_{rot}(E_{min})$) the c/a constraint.

V/V_0	E (c/a=1.610)	θ_{rot}(1.610)	c/a for Emin	Emin	$\theta_{rot}(E_{min})$
0.9707	-6250.5389	0.259 deg	1.634	-6250.7528	0.339 deg
0.9497	-6249.3460	0.540 deg	1.649	-6249.6401	0.836 deg
0.9439	-6248.7450	0.667 deg	1.591	-6249.3578	1.556 deg
0.8368	-6243.5107	12.041 deg	1.567	-6243.9755	12.810 deg

From these results we observe that unconstraining the c/a value during the compression has a rather small effect on the consequent energetic and structural evolution of the compressed NPSL, supporting the adequacy of our constrained simulation results.

DOI: 10.1038/NMAT3923

S.3 The Birch equation of state (EOS)

The equation of state (EOS) may be derived by expanding the energy, E,

$$E(V) = e_0 + e_1 \varepsilon + e_2 \varepsilon^2 + e_3 \varepsilon^3 + \ldots \quad , \qquad (1)$$

as a function of volume through the Eulerian strain,

$$\varepsilon = [(V/V_r)^{-2/3} - 1]/2, \qquad (2)$$

relative to the volume, V_r at a chosen reference point. While the reference point is commonly that of zero pressure, it need not be so, and our notation will reflect this (e.g., P_r rather than P_0). This is particularly important in fitting higher compression results to an EOS when there is a higher pressure phase that may not exist at zero pressure. This higher pressure phase will have its own unique set of elastic properties and it is convenient to choose a reference state in the regime of pressure and volume in which the material phase exists.

One approach in fitting a data set to the EOS of the form given in Eq. 1 is to simply use the coefficients e_0, e_1, e_2 , e_3 , …as the fitting constants. These constants can be related to physical properties of the material by using constitutive relations and the EOS may then be expressed in terms of these (physically meaningful) variables. Alternatively, and more commonly, the EOS can be expressed from the beginning in terms of constants that characterize the material and these can be used as the fitting constants. To relate the fitting constants of Eq. 1 in terms of material properties, use is made of the fundamental equations

$$P = -dE/dV \ , \qquad (3)$$

relating changes in energy to pressure-driven changes in volume; the bulk modulus,

$$B = -V\, dP/dV\,, \qquad (4)$$

expressing the elastic response of a material subject to pressure and volume changes; and the first and higher pressure derivatives of the bulk modulus (e.g. , the first is B' = dB/dP and second B''=dB'/dP). Series expressions for all of these properties, are found through differentiation of the energy E(V) (Eq. 1). The fitting constants are found by requiring that these expansions, E(V), P(V), B(V) , B'(V), B''(V), … , give the corresponding material constants E_r, P_r, B_r, Br, B_r'' , … when the volume V approaches the reference volume V_r. These fitting variables, e.g. (E_r, P_r, B_r), represent values of the EOS evaluated at the reference volume, V_r . If a different reference volume,V_{r2}, had been chosen, the fitting constants {E_{r2}, P_{r2}, B_{r2}} will represent the corresponding physical quantities at the new reference point but the two EOS curves (e.g. E (V) vs V) will lay on top of one another. If the expressions of the second EOS (with reference volume V_{r2}) are evaluated at the first volume V=V_r , one should get the same (E_r, P_r, B_r) as found in the initial fit.

The 3rd order Birch EOS (ref 1), for a reference state of zero pressure, that results from the above procedure is

$$E(E_0, V_0, B_0, B_0', \varepsilon) = E_0 + (9/2)\, \varepsilon^2\, B_0 V_0\, [1 + (B_0' - 4)\, \varepsilon]\,, \qquad (5)$$

$$P(B_0, B_0', \varepsilon) = 3\, \varepsilon\, B_0 [\, 1 + (3/2)\, (B_0' - 4)\, \varepsilon\,]\, (1 + 2\varepsilon)^{5/2}\,, \qquad (6)$$

with an implicit volume, V, dependence through the Eulerian strain ε (Eq. 2). The expression for energy (Eq. 5) is used to describe the lower compression results of this work where one has the set of energies, E({V_n}), computed from theory for a range of

DOI: 10.1038/NMAT3923

pressure. The fitting constants are the zero pressure bulk modulus, B_0, and its first pressure derivative, B_0' , which are found to be B_0 = 16.7 GPa, and B_0' = -17.5. The negative value of B_0' indicates a pressure-induced softening.

The description of the higher compression results, which exhibits a phase change, makes use of a modified Birch EOS in which the reference volume is chosen as the first point of compression that exhibits the new phase. As discussed earlier, other choices of reference volume will give equally good results. This form of the EOS is derived in the same manner as the ordinary Birch EOS (see Eqs 1-4 and related discussion) but the condition of zero pressure at the reference volume is not imposed (ref 2 gives this modified EOS to 3rd order in the energy).

An adequate description of the present results is given by the 2nd order (i.e. 2nd order energy expansion) modified Birch EOS, which has the form

$$E(E_r, V_r, P_r, B_r, \varepsilon_r) = E_r + 9/2\, V_r\, \varepsilon_r\, [\, B_r\, \varepsilon_r + 1/3\, P_r (2 - 5\, \varepsilon_r)\,] \quad (7)$$

$$P(P_r, B_r, \varepsilon_r) = [3\, B_r\, \varepsilon_r + P_r (\, 1 - 5\varepsilon_r)\,]\, (1 + 2\varepsilon_r)^{2.5} \quad (8)$$

$$B(V_r, P_r, B_r, \varepsilon_r) = [\, B_r\, (1 + 7\, \varepsilon_r) - 35/3\, P_r\, \varepsilon_r \,]\, (1 + 2\varepsilon_r)^{2.5} \quad (9)$$

$$B'(P_r, B_r) = 4 - (35/9)\, P_r/B_r \quad (10)$$

Note that the first pressure derivative of the bulk modulus does not have a volume dependence in the 2nd order theory.

If the reference state is that of zero pressure, Pr = P_0 = 0, the above expressions reduce to the ordinary 2nd order Birch EOS. In the fits of the higher strain region, the chosen reference volume, (corresponding to the first point at which the new phase first appears) is V_r = 23075.2 Å^3. When results are presented as a function of V/V_0, where V_0

is the volume at zero pressure, the beginning of the high-compression interval corresponds to $V_r/V_0 > 0.94$.

The results of this fit are E_r= -6248.98 eV, P_r = 0.324 GPa, and B_r = 0.347 GPa. The first pressure derivative of the bulk modulus is B_r'=0.37 indicating that the bulk modulus increases with pressure in contrast to pressure-induced softening in the low-strain region.

1. Birch, F., Finite Strain Isotherm and Velocities for Single-Crystal and Polycrystalline NaCl at High Pressures and 300° K. *J. Geophys. Res.* **83**, 1257-1268 (1978).

2. Sata, N., Guoyin, S., Rivers, M. L. & Sutton, S. R., Pressure-volume equation of state of the high-pressure *B*2 phase of NaCl. *Phys. Rev. B.* **65**, 104114-1, 104114-7 (2002).

DOI: 10.1038/NMAT3923

S.4 Intralayer and interlayer NP rotations

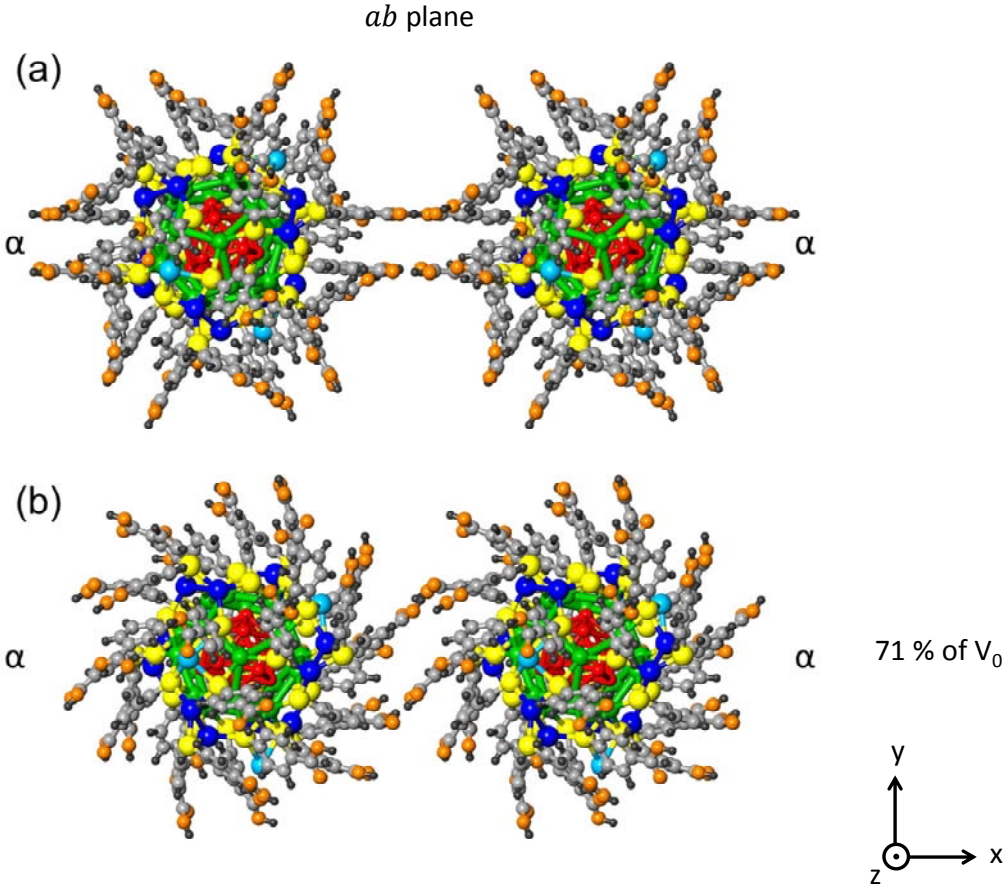

Figure S2(a)

Figure S2(a) : Configuration of two neighboring nanoparticles, both located in the same layer of the superlattice**.** The view is in the normal direction to the (**a**,**b**), or (x,y) plane (see Fig.1a of the manuscript) . The views in (a), upper row, and (b) lower row, corresponds to the initial state, with V/V_0 =1, and the rotated state at the end of the compression process (V/V_0 =0.71)., respectively; See also Fig. 2(b) of the manuscript. Note the equal sense of rotations of the two nanoparticles.

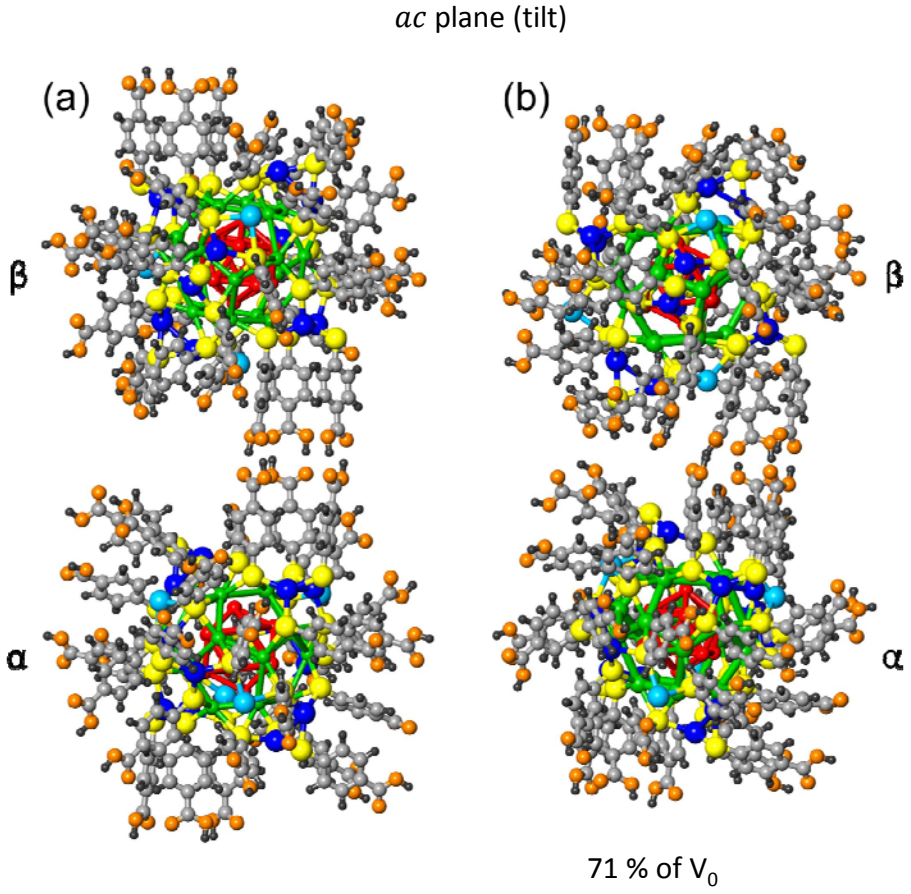

Figure S2(b)

Figure S2(b) : Configuration of two neighboring nanoparticles, located in neighboring layers of the superlattice, denoted as α and β**.** The view is in the normal direction to the (**a**,**c**) plane (see Fig. 1 of the manuscript). The views in the left column (a), and the right coulmn (b), correspond, respectively, to the initial state (V/V_0 =1) and the rotated state at the end of the compression process (V/V_0 =0.71). Note the opposite senses of the cluster rotations between the two layers. For a view normal to the (**a**,**b**) plane (as in Fig. S2(a)) see Figs. S2(c,d)

DOI: 10.1038/NMAT3923

Figure S2(c) $V/V_0 = 1$

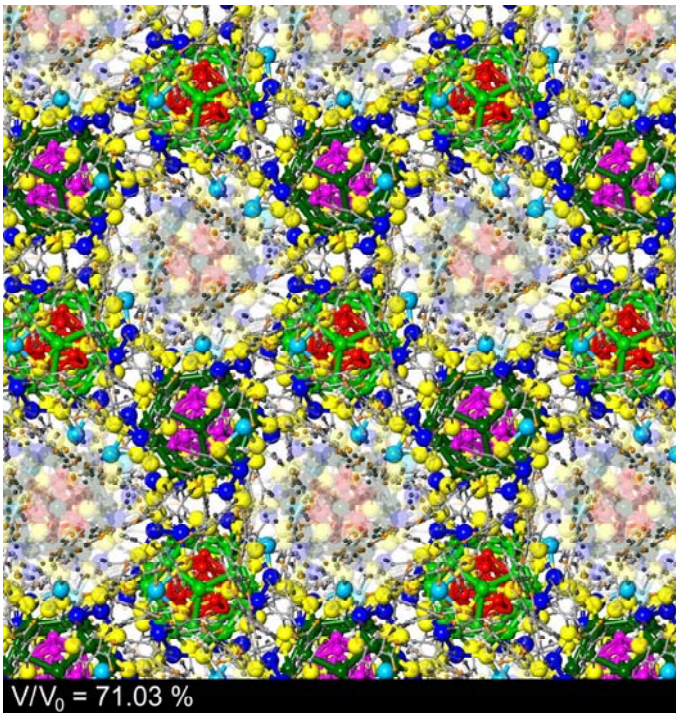

Figure S2(d) $V/V_0 = 0.71$

Figures S2(c,d): Configurations of the superlattice viewed normal to the **(a,b)** [or (x,y) plane] plane (as in Fig. S2(a). The configuration in (C) corresponds to $V/V_0 = 1.0$ and the one in (d) corresponds to the end of the compression process at V/V0 =0.71. The graphic presentation in this figures is similar to that shown in Fig. 1(c) of the manuscript. As described in the manuscript the Na_4Ag_{44} (p-MBA)$_{30}$ NPs are organized in layers (with each of the layers consisting of identical NPs. On the other hand the NPs in neighboring layers (denoted as α and β NPs) are related by a mirror reflection in the x=0 plane (i.e. (x, y, z) → (-x, y, z)) followed by a translation by **c**/2. The layers are stacked as in a face-centered-cubic (fcc) lattice (with the 3-layer stacking sequence denoted as A, B,C). The NPs in each layer form a (filled) hexagonal lattice. In Figs. S2(c) and S2(d) the fcc A,B, and C layers are distinguished by coloring the Ag_{20} dodecahedron: light green (A), darker green (B), and the C) is populated by the faded clusters. The NPs in neighboring layers are distinguished also by the coloring of the 12 Ag atom inner-shell icosahedron which is colored red in the A layer, and pink in the B layer. In the equilibrium configuration (Fig. S2(c)) the clusters in the A and B layers are mirror reflection of each other. Comparison of the cluster configurations in Fig, S2(c) and Fig. S2(d) reveals that the cluster in layer A of Fig. S2(d) are rotated anti-clockwise with respect to the corresponding clusters in Fig. S2(c). On the other hand the clusters in the B layer of Fig. S2(d) are found to be rotated in the clockwise direction with respect to the corresponding clusters in Fig. S2(c).

DOI: 10.1038/NMAT3923

S.5 Torsion angles plotted versus the compression parameter V/V_0

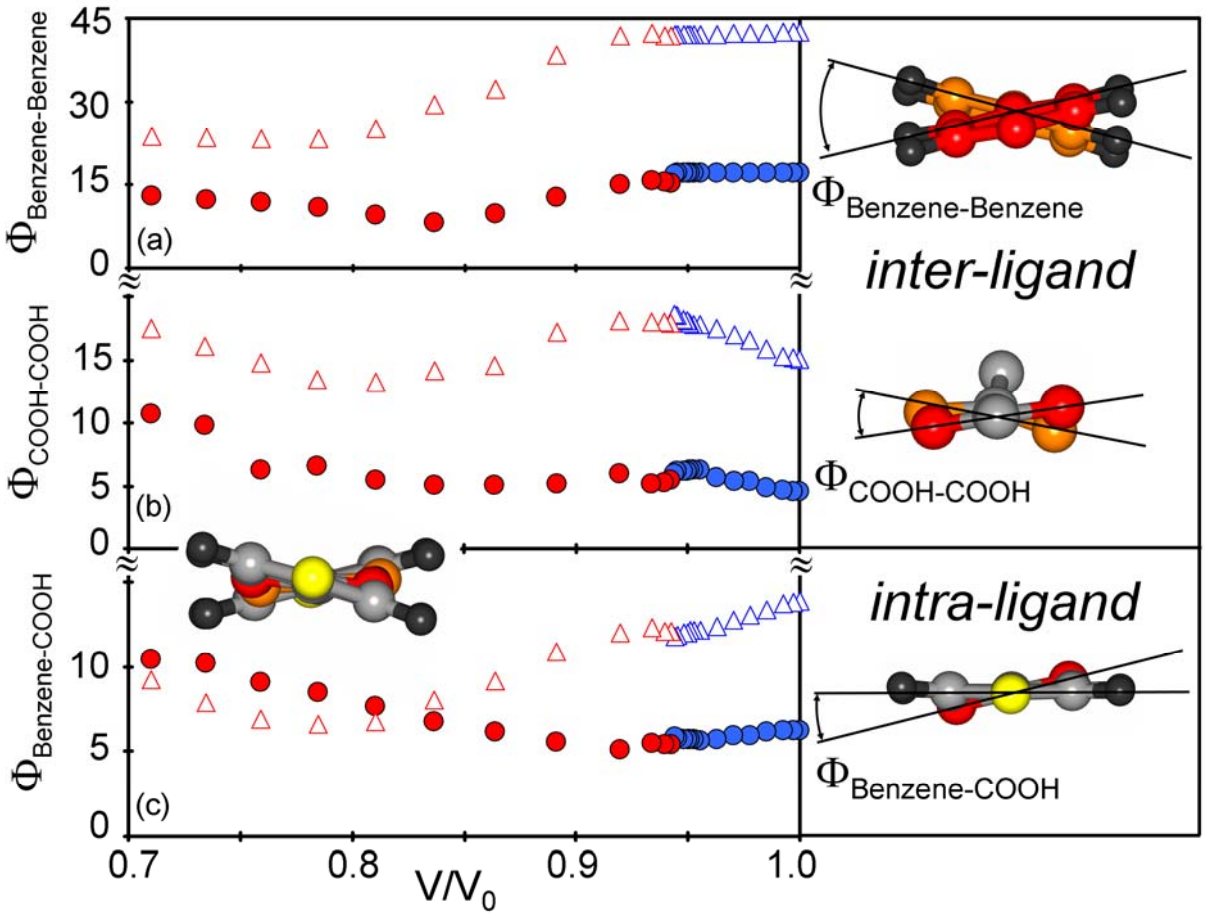

Figure S3

Figure S3. Interligand and intraligand torsion angles plotted versus the compression parameter $V/V_0 \leq 1$. Blue and red symbols correspond to the low-strain and high-strain compression intervals. Circles denotes angles for ligands connecting NPs located in the same layer, and the triangles correspond to ligands connecting NPs in neighboring layers. The inset on the left in (c) is a (S-to-S) view along the axix connecting the two sulfur

atoms, each anchoring a p-MBA ligand to a neighboring nanoparticle. In each of the insets on the right we isolate a particular component of the overall S-to-S view, serving to define the torsion angle whose variation we show in the corresponding panel.

DOI: 10.1038/NMAT3923

S.6 Compression-induced changes in the structure of the Na_4Ag_{44} (p-MBA)$_{30}$ nanoparticle in the superlattice

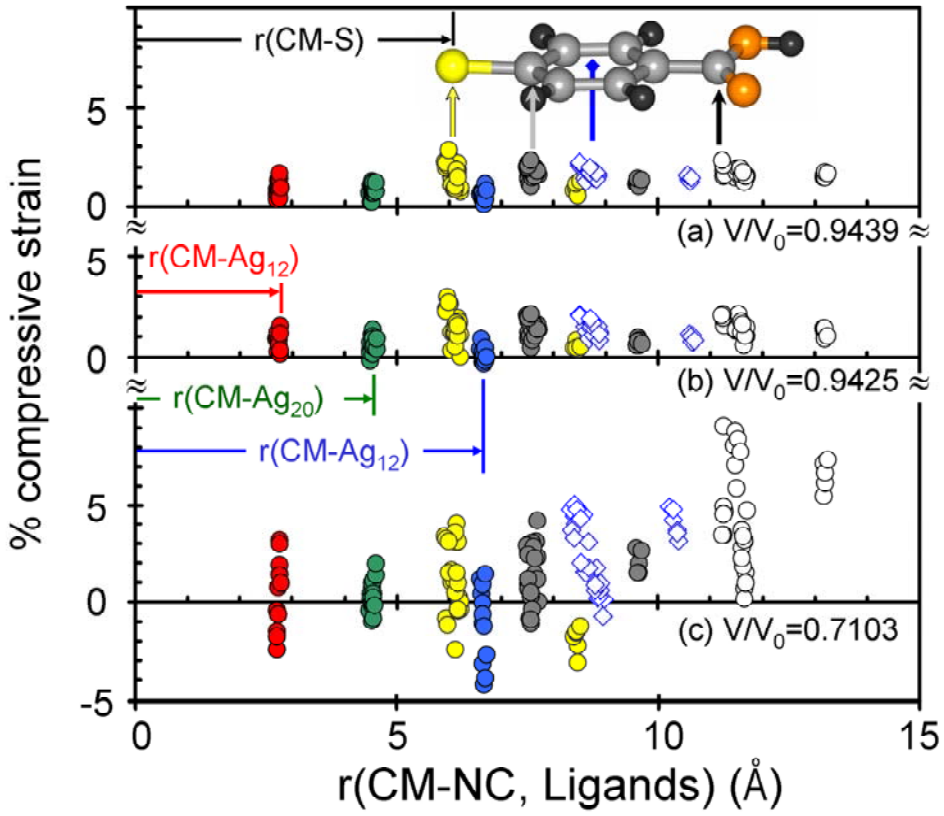

Figure S4

Figure S4. Compression-induced changes in the radial distances of atoms (grouped into radial shells, relative to the NP's center of mass, CM) in the Na_4Ag_{44} (p-MBA)$_{30}$ nanoparticle; positive values correspond to contraction of the radial distance, and negative values indicate radial expansion. The changes are given relative to their value in the uncompressed state (that is expressed as the % compression-induced strain). These compression induced-strains are shown for three volume compressions (V/V_0) of the superlattice:

(a) V/V_0= 0.9439, the last point of the low-strain region before the pressure-induced phase change.;

(b) V/ V_0= 0.9425, the first point of the high-strain region at which the phase change occurred.

(c) V/ V_0= 0.7103, the last and most compressed state.

As indicated in the figure, the (NP, Ligand) members discussed are: the atoms in the three silver shells (red, green and blue) of the nanoparticle, the sulfur atom (yellow) of the p-MBA ligand, the phenyl ring carbon atom bonded to S, the CM of the phenyl group, and the carbon atom of the carboxyl group. Note that for every group of points corresponding to the p-MBA ligand, there is a smaller group of the same type about 2 Å further out, corresponding to the ligands that are bonded to the six mount of the silver nanoparticle [see: Desireddy, A. et. al. Ultrastable silver nanoperticles. *Nature* **501** 399-402 (2013)].

.

DOI: 10.1038/NMAT3923

S.7 Calculation of cluster Rotations (Fig. 3(j))

Analysis of cluster rotation

Step 1. Calculate unit position vector of each Ag atom with respect to the center of core Ag_{12}.

$$\mathbf{r}_i = \frac{\mathbf{R}_i - \mathbf{R}_{\mathrm{CM}}}{|\mathbf{R}_i - \mathbf{R}_{\mathrm{CM}}|}$$

Step 2. Calculate the cross product of unit position vectors before and after compression.

$$\mathbf{A}_i{}^{(n)} = \mathbf{r}_i{}^{(n)} \times \mathbf{r}_i{}^{(0)}$$

Step 3. Calculate the rotation axis using the formula below:

$$\mathbf{a}^{(n)} = \frac{\sum_i \mathbf{A}_i{}^{(n)}}{\left|\sum_i \mathbf{A}_i{}^{(n)}\right|}$$

Step 4. Calculate the component of the unit position vector perpendicular to the rotation axis.

$$\mathbf{r}_{i,\perp}{}^{(n)} = \frac{\mathbf{r}_i{}^{(n)} - \left(\mathbf{r}_i{}^{(n)} \cdot \mathbf{a}^{(n)}\right)\mathbf{a}^{(n)}}{\left|\mathbf{r}_i{}^{(n)} - \left(\mathbf{r}_i{}^{(n)} \cdot \mathbf{a}^{(n)}\right)\mathbf{a}^{(n)}\right|}$$

Step 5. Calculate the rotation angles of Ag atom using the formula below:

$$\varphi_i{}^{(n)} = \sin^{-1}\left(\left|\mathbf{r}_{i,\perp}{}^{(n)} \times \mathbf{r}_{i,\perp}{}^{(0)}\right|\right)$$

Step 6. Calculate the cluster rotation angle using the formula below:

$$\varphi^{(n)} = \frac{\sum_i \varphi_i{}^{(n)} \left|\mathbf{r}_{i,\perp}{}^{(n)}\right|}{\sum_i \left|\mathbf{r}_{i,\perp}{}^{(n)}\right|}$$

For definitions of the vectors mentioned above and the rotation angle, see the figure on the next page.

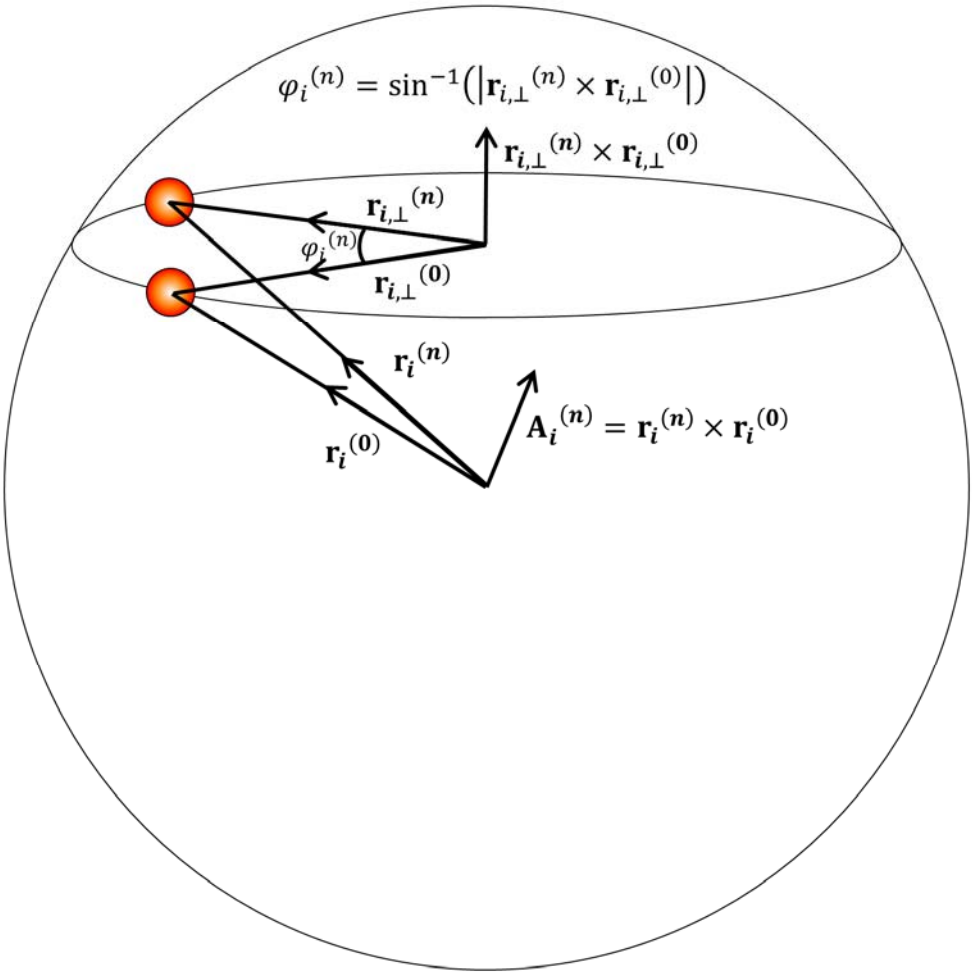

Figure S5

Figure S5. Definition of variables appearing in the description of the calculation of the cluster rotation angle.